Journal of Neuroscience Research 00:00–00 (2016)

Cellular and Molecular Neuroscience

Extracellular ATP Induces Graded Reactive Response of Astrocytes and Strengthens Their Antioxidative Defense In Vitro

Marija Adzic,[1,2] Ivana Stevanovic,[3] Natasa Josipovic,[1] Danijela Laketa,[1] Irena Lavrnja,[4] Ivana M. Bjelobaba,[4] Iva Bozic,[4] Marija Jovanovic,[4] Milena Milosevic,[1,2] and Nadezda Nedeljkovic[1]*

[1]Institute for Physiology and Biochemistry, Faculty of Biology, University of Belgrade, Belgrade, Serbia
[2]Centre for Laser Microscopy, Faculty of Biology, University of Belgrade, Belgrade, Serbia
[3]Institute for Medical Research, Military Medical Academy, Belgrade, Serbia
[4]Institute for Biological Research "Sinisa Stankovic,", University of Belgrade, Belgrade, Serbia

It is widely accepted that adenosine triphosphate (ATP) acts as a universal danger-associated molecular pattern with several known mechanisms for immune cell activation. In the central nervous system, ATP activates microglia and astrocytes and induces a neuroinflammatory response. The aim of the present study was to describe responses of isolated astrocytes to increasing concentrations of ATP (5 μM to 1 mM), which were intended to mimic graded intensity of the extracellular stimulus. The results show that ATP induces graded activation response of astrocytes in terms of the cell proliferation, stellation, shape remodeling, and underlying actin and GFAP filament rearrangement, although the changes occurred without an apparent increase in GFAP and actin protein expression. On the other hand, ATP in the range of applied concentrations did not evoke IL-1β release from cultured astrocytes, nor did it modify the release from LPS and LPS+IFN-γ–primed astrocytes. ATP did not promote astrocyte migration in the wound-healing assay, nor did it increase production of reactive oxygen and nitrogen species and lipid peroxidation. Instead, ATP strengthened the antioxidative defense of astrocytes by inducing Cu/ZnSOD and MnSOD activities and by increasing their glutathione content. Our current results suggest that although ATP triggers several attributes of activated astrocytic phenotype with a magnitude that increases with the concentration, it is not sufficient to induce full-blown reactive phenotype of astrocytes in vitro.

Key words: ATP; reactive astrocytes; reactive gliosis; antioxidative defense; IL-1β

INTRODUCTION

Adenosine triphosphate (ATP) plays a fundamental role inside the cells as the energy transfer molecule and phosphate group donor (Lipmann, 1941). Outside the cells, ATP acts as a versatile signaling molecule, acting at two classes of purinoceptors, ligand-gated P2X and G-protein–coupled P2Y receptors. Seven P2XR subunits assemble to form homomeric or heteromeric receptor channels activated by ATP (Khakh and North, 2012). Eight P2Y receptors have been identified exhibiting differential sensitivity to ATP ($P2Y_{2,4,11}$), ADP ($P2Y_{1,12,13}$), and other nucleotides (Abbracchio et al., 2006). ATP-induced signaling is short-lived and terminated by an

SIGNIFICANCE

The study assesses how cortical astrocytes in vitro respond to extracellular ATP in the concentration range of 5 μM to 1 mM. Dose–response relationships from exposure to ATP, in terms of astrocyte proliferation, stellation, and shape remodeling, have been viewed as manifestations of astrocytes' reactive response. On the other hand, the stimulatory response of astrocytes in terms of their antioxidative defense has been interpreted as an indicator of their adaptive response to ATP. The dual pattern of astrocytic response to ATP may have significant implications in a wide range of neurological conditions associated with neuroinflammation.

Grant information: This work was supported by Ministry of Education, Science and Technological Development Project No. III41014 (http://www.mpn.gov.rs). Marija Adzic was supported by DAAD Akademischer Neuaufbau Sudosteuropa.

*Correspondence to: Nadezda Nedeljkovic, Institute for Physiology and Biochemistry, Faculty of Biology, University of Belgrade, Studentski trg 3, 11001 Belgrade, Serbia. E-mail: nnedel@bio.bg.ac.rs

Received 20 March 2016; Revised 6 September 2016; Accepted 7 September 2016

Published online 00 Month 2016 in Wiley Online Library (wileyonlinelibrary.com). DOI: 10.1002/jnr.23950

enzymatic degradation of ATP, catalyzed by the ectonucleotidase enzyme chain. Ectonucleoside triphosphate diphosphohydrolases (E-NTPDases) degrade ATP and ADP, while ecto-5′-nucleotidase hydrolyzes AMP to adenosine. Adenosine acts at its own P1 receptors (Burnstock et al., 2011; Fredholm et al., 2011) to induce cellular responses.

ATP is released from neurons (White, 1977; Pankratov et al., 2006; Fields, 2011), astrocytes (Koizumi, 2010), and microglia (Imura et al., 2013; George et al., 2015) through multiple pathways (Bodin and Burnstock, 2001). Since P2 receptors display widespread cellular distribution in the brain (Burnstock et al., 2011), multiple roles have been attributed to the extracellular ATP, including neurotransmission, neuromodulation, and trophic actions. Moreover, there is growing evidence for a rapid increase in the extracellular ATP levels upon noxious brain conditions, such as trauma (Wang et al., 2004; Davalos et al., 2005; Franke et al., 2006) and hypoxia/ischemia (Juranyi et al., 1999; Melani et al., 2005). In such conditions, ATP acts as a danger-associated molecular pattern (DAMP) (Bours et al., 2006, 2011; Rodrigues et al., 2015), able to sustain its own release and preserve the enhanced levels by acting at P2X7R and P2Y1R at neurons, microglia, and astrocytes (Pankratov et al., 2006; Kim et al., 2007; Bennett et al., 2012). By acting at low-affinity P2X7R, ATP controls and directs the neuroinflammatory response of overactivated microglia (Koizumi et al., 2013; Idzko et al., 2014) and induces release of IL-1β, essential for morphological and functional activation of astrocytes (Liu et al., 2000; Dunn et al., 2002; Cahill and Rogers, 2008; Silverman et al., 2009; He et al., 2015). The actions of ATP through P2Y1R promote reactive astrogliosis upon mechanical injury (Franke et al., 2001), ischemic conditions (Sun et al., 2008), or Alzheimer disease (Delekate et al., 2014).

Reactive astrogliosis is a common response of astrocytes to noxious stimuli, characterized by hypertrophy and hyperplasia of astrocytes (Sofroniew, 2009) and their migration to the site of injury, resulting in loss of non-overlapping domain organization and formation of a glial scar (Oberheim et al., 2008). While in physiological conditions astrocytes produce growth factors and antioxidative molecules, which support neuronal stability (Shih et al., 2003), reactive astrocytes release proinflammatory mediators and reactive oxygen (ROS) and nitrogen species (RNS), which promote inflammation (Farina et al., 2007; Kim et al., 2010; Steele et al., 2013).

The large body of evidence obtained in different experimental models and human specimens indicates that the process of reactive astrogliosis is not an all-or-none response leading to the formation of a glial scar, but a broad continuum of alterations in the cells' morphology and function (Sofroniew, 2009). Given that ATP acts both as a trophic factor and DAMP molecule, the aim of our study was to assess responses of astrocytes to a range of ATP concentrations intended to mimic graded intensity of the stimulus. We demonstrate that ATP induced the graded response of astrocytes in terms of proliferation and shape remodeling. On the other hand, it did not promote IL-1β release and migration of activated astrocytes but instead strengthened their antioxidative capacity by inducing superoxide dismutase (SOD) activity and increasing their glutathione (GSH) content.

MATERIALS AND METHODS

Chemicals

Glucose, poly-L-lysine (PLL), Trypsin, EDTA, Triton™ X-100, adenosine 5′-triphosphate disodium salt (ATP), bovine serum albumin (BSA), normal goat serum, 3-(4,5-dimethyl-2-thiazolyl)−2,5-diphenyl-2H-tetrazolium bromide, dimethyl sulfoxide (DMSO), 2,2'-azino-bis(3-ethylbenzothiazoline-6-sulphonic acid) substrate, paraformaldehyde (PFA), protease inhibitor cocktail, probenecid, and Mowiol bedding medium were all purchased from Sigma-Aldrich (St. Louis, MO). Leibovitz's L-15 medium, penicillin/streptomycin, fetal bovine serum (FBS), Dulbecco's modified Eagle's medium (DMEM), and phalloidin conjugated AF 568 were obtained from Gibco (Invitrogen; Carlsbad, CA). A BCA protein assay kit was purchased from Pierce Biotechnology (Rockford, IL). The Mini ELISA Development Kit for IL-1β was a product of Peprotech (Rocky Hill, NJ). Avidin-HRP conjugate was purchased from eBioscience (Frankfurt, Germany). 4,6-Diamidino-2-phenylindole (DAPI) was purchased from Molecular Probes (Eugene, OR). Annexin V-FITC was obtained from Santa Cruz (Dallas, Texas), while propidium iodide (PI) was purchased from BD Pharmingen (San Diego, CA). Donkey anti-rabbit AF 488, donkey anti-mouse AF 488, and donkey anti-goat AF 643 antibodies were purchased from Invitrogen (Carlsbad, CA).

Antibody Characterization

For a list of all primary antibodies used, see Table I. Anti-Iba1 and anti-CNPase antibodies were used on primary mixed cultures containing neurons, astrocytes, oligodendrocytes, and microglia, where they showed positive immunofluorescence labeling. The anti-GFAP antibody stained a pattern of cellular morphology and distribution as previously described (Brisevac et al., 2015). Anti-Ki-67 antibody showed an expected prominent staining pattern localized in nuclei, but not in the cytoplasm. The omission of the primary antibody in the protocol resulted in the absence of specific fluorescence. In Western blot analysis, the anti-IL-1β antibodies recognized a single band of 17 kDa of recombinant rat IL-1β (200 ng/ml, R&D Systems, 501-RL). Both anti-GFAP and anti-β-actin antibodies detected a single band at 55 and 42 kDa, respectively.

Animals

One to two-day-old rat pups of the Wistar strain from the local colony were used in the study. All animal procedures were carried out in compliance with Directive 86/609/EEC on the protection of animals used for experimental and other scientific purposes and were approved by the Ethical Committee for the Use of Laboratory Animals, Institute for Biological Research "Sinisa Stankovic"(no. 2-34/11). A total of 30 animals of both sexes were used for primary astrocyte culture isolation for the purposes of this study.

TABLE I. Primary Antibodies Used

Antibody name	Description of immunogen	Source, host species, catalog no., clone or lot no., RRID	Dilution used
Anti-Iba1	Synthetic peptide: C-TGPPAKKAISELP, corresponding to amino acids 135-147 of Human Iba1	Abcam, goat polyclonal, ab5076, RRID: AB_2224402	1:500 in NDS/BSA/PBS (ICH)
Anti-Ki-67	Synthetic peptide conjugated to KLH derived from within residues 1200–1300 of Human Ki67	Abcam, rabbit polyclonal, ab15580, RRID: AB_443209	1:500 in NDS/BSA/PBS (ICH)
Anti-GFAP	GFAP isolated from cow spinal cord	DAKO, rabbit polyclonal, Z0334, RRID: AB_10013382	1:500 in NDS/BSA/PBS (ICH); 1:7,000 in TBST (WB)
Anti-myelin CNPase	Purified, human myelin CNPase	EMD Millipore, mouse monoclonal, NE1020, clone SMI-91, RRID: AB_10682518	1:200 in NDS/BSA/PBS (ICH)
Anti-β-actin	AC-74 hybridoma: the fusion of mouse myeloma cells and splenocytes from BALB/c mice immunized with a slightly modified synthetic b-cytoplasmic actin N-terminal peptide	Sigma-Aldrich, mouse monoclonal, A5316, RRID: AB_476743	1:5,000 in TBST (WB)
Anti-IL-1β conjugated HRP	*E. coli*–derived recombinant rat IL-1 beta/IL-1F2	R&D Systems, goat polyclonal, BAF501, RRID: AB_2124741	1:2,000 in TBST (WB)

Primary Cortical Astrocyte Culture

Cerebral cortices were dissected, and meninges were peeled off in ice-cold phosphate-buffered saline (PBS). Briefly, after brain dissection, the cortices were isolated and mechanically dissociated under sterile conditions in Leibovitz's L-15 isolating medium supplemented with 2 mM L-glutamine, 100 IU/ml penicillin, 0.1 mg/ml streptomycin, and 0.1% BSA. After two centrifuge steps at 500*g* for 4 min, the cell suspension was passed through 21 G and 23 G sterile needles (to remove residual tissue aggregates). An additional centrifugation step at 500*g* for 4 min was followed by cell resuspension in DMEM with the addition of 10% heat-inactivated FBS, 25 mmol/l glucose, 2 mmol/l L-glutamine, 1 mmol/l sodium pyruvate, 100 IU/ml penicillin, and 100 μg/ml streptomycin. Cells were subsequently seeded in 25 cm^2 tissue culture flasks and grown at 37°C in a humidified incubator with 5% CO_2/95% air, and culture medium was replaced every third day. After 6 to 8 days in culture, primary microglia and oligodendrocytes were removed by vigorous shaking at 400 rpm for 16 to 20 hr on a plate shaker (Perkin Elmer, Turku, Finland). Adherent primary astrocytes were washed with PBS, trypsinized (0.25% trypsin and 0.02% EDTA) and replated at a density of 1.5×10^4 cells/cm^2, and maintained to reach confluence. Each cell culture was prepared from single animal cortices.

Primary Culture Characterization and Assessment of Purity

Primary cortical astrocyte cultures prepared with multiple passages consisted of virtually pure $GFAP^+$ cells (98.6%), as demonstrated by immunostaining according to the afterward-listed protocol. Images of microscopic fields (five fields per coverslip) were captured on the confocal laser scanning microscope (LSM 510, Carl Zeiss GmbH, Jena, Germany) equipped with Ar Multi-line (457, 478, 488, and 514 nm) and HeNe (543 and 633 nm) lasers, using 40× DIC oil and 63× DIC oil objectives and monochrome camera AxioCam ICm1camera (Carl Zeiss GmbH, Germany). Cells were counted by using ImageJ (Cell counter plugin). The presence of $GFAP^+$, $Iba1^+$, and $CNPase^+$ cells was expressed relative to the total number of cells in the fields (DAPI staining) ± standard error of the mean (SEM). GFAP-expressing cells constituted the vast majority of cells in the cultures (98.6%), while the remaining cells, based on Iba1 immunolabeling, represented a microglial fraction of less than 2% of the total cell number. CNPase-expressing oligodendrocytes were not detected. The omission of the primary antibodies resulted in the absence of labeling.

Immunocytochemistry

If not otherwise stated, immunocytochemical labeling was conducted according to the following protocol: cells seeded on PLL-coated glass coverslips (25 mm) were fixed in 4% PFA for 20 min and rinsed in PBS. Cells were then permeabilized in 0.1% Triton X-100 and blocked in 10% NDS, 1% BSA in 0.01 M PBS for 60 min at room temperature (RT). For double immunolabeling, primary antibodies were applied in a sequential manner, overnight at 4°C in 1% NDS and 1% BSA solution (for dilutions, see Table I). Appropriate secondary fluorescence-labeled antibodies were applied for 2.5 hr in the dark, at RT and 1:200 dilutions. After the washing, coverslips were incubated for 10 min with a nuclear counterstain (DAPI, 1:4,000), washed again thoroughly, and mounted on microscopic slides using Mowiol medium.

Treatments

Cells in culture were synchronized by shifting the serum concentration to 0.1% FBS, 24 hr before the experiment. On

the day of the experiment, the medium was replaced with normal medium (10% FBS) containing ATP (5 μM to 1 mM), and cells were kept for the indicated period of time (15 min to 48 hr). Cultures grown in normal medium without ATP were used as a control.

For IL-1β enzyme-linked immunosorbent assay (ELISA) measurements, cultures were prepared as described and treated with LPS (1 μg/ml), alone or in a combination with IFN-γ (100 U/ml) or ATP (1mM), for 24 hr.

Microculture Tetrazolium Assay

Microculture tetrazolium (MTT) assay is a colorimetric assay for assessing cell viability by evaluating total mitochondrial activity. Astrocytes (2×10^4 cells/cm^2) were grown on the 24-well plate until they reached 80% confluence and were subsequently treated with ATP (5 μM to 1 mM) for 24 hr. After the treatment, the media were discarded and 200 μl of MTT solution was added to each well in a final MTT concentration of 1 mg/ml. Formazan generated by total mitochondrial activity was dissolved in 750 μl of DMSO, homogenized, and each sample was placed in triplicate on the 96-well plate. Optical density was measured at 540 nm with a microplate reader (LKB 5060-006, Vienna, Austria) with the correction set at 670 nm. The total mitochondrial activity of treated cells was expressed as a percentage of control cultures. Results are presented as mean percentage ± SEM from two different cell culture preparations.

Flow Cytometry Analysis and Annexin V/PI Staining

For flow cytometry quantification of cell survival, astrocytes were seeded at two different densities (2×10^4 cells/cm^2 and 4×10^4 cells/cm^2), thus allowing one group to reach the complete confluence, while at the same time, the other group reached 70% to 80% confluence. Both groups were treated at the same time with the indicated concentration of ATP, and measurements were performed 4 and 24 hr after. The early apoptotic cells translocate their phosphatidylserine to the outer membrane surface, which could then be recognized by Annexin V. The late apoptotic and necrotic cells become permeable to PI. According to the manufacturer's instructions, we performed the double staining with Annexin V-FITC (Santa Cruz, Dallas, TX) and PI (BD Pharmingen, San Diego, CA). Cells negative for both dyes were considered viable. Analyses were performed in quadruplicate (CyFlow Space Partec, Partec GmbH, Munster, Germany), and PartecFloMax software (Partec GmbH, Munster, Germany) was used for data acquisition and analysis. Results are presented as mean percentage of total cell population.

Cell Proliferation Assay

Astrocytes (2×10^4 cells/cm^2) were plated on PLL-coated glass coverslips (25 mm). Cultures were maintained as described. Cultures reached 80% confluence when treated. Control cultures and cultures treated with ATP (5 μmol/L to 1 mmol/L) were left to grow for the indicated period of time and then were immunocytochemically labeled for Ki67 and counterstained with DAPI using the above-described protocol. The omission of the primary antibody resulted in the absence of labeling. Cells from six to eight fields per each coverslip were captured on Carl Zeiss AxioObserver A1 inverted microscope (A-Plan 10× objective) by EM512 CCD Digital Camera System (Evolve, Photometrics). Cells were counted using the ImageJ software package (http://imagej.nih.gov/ij/download.html), and the number of Ki67-positive cells was expressed as a mean percentage (± SEM) of total cell number (DAPI-positive), from three separate cell culture preparations and independent treatments.

The proliferation assessment using Ki67/DAPI labeling was applied for cultures subjected to the ATP-treated wound-healing assay experiment. Treated and control cultures were prefixed at indicated time points (0–48 hr), and the immunofluorescence protocol was further applied as described.

Morphometric Analysis

Astrocytes (2×10^4 cells/cm^2) were plated and treated with ATP (10 μM to 1 mM), and cell morphology was analyzed. In each treatment group, cells from at least six fields per culture dish (35 mm), from two independent culture preparations, were captured on an AxioObserver A1 inverted microscope (A-Plan 10× objective) by EM512 CCD Digital Camera System (Evolve, Photometrics). Images were analyzed using the ImageJ software package (National Institutes of Health, Bethesda, MD). Mean cell surface area was determined according to the instructions (http://imagej.net/Category:Tutorials) and was expressed in micrometers squared ± SEM (615 pixels/mm). Stellation induced by ATP treatment was quantified using the same software package, by counting the number of stellate cells out of the total number of cells (mean percentage ± SEM) in two different culture preparations. Since the vast majority of cells in control culture exhibit epithelioid morphology without processes, ATP-induced stellation was arbitrarily defined as the appearance of more than three processes per cell.

Actin and GFAP Fluorescence Staining

Actin and GFAP were labeled using the phalloidin fluorescence and anti-GFAP immunofluorescence staining, followed by DAPI counterstaining. Images of GFAP/phalloidin double-stained astrocytes were obtained on the confocal laser scanning microscope (LSM 510, Carl Zeiss GmbH, Jena, Germany) using Ar Multi-line (457, 478, 488, and 514 nm) and HeNe (543 and 633 nm) lasers, and 40× DIC oil and 63× DIC oil objectives.

Wound-Healing Assay

Astrocyte cultures (2×10^4 cells/cm^2) were maintained until complete confluence was reached. Wound-healing assay was performed essentially by following the protocols previously described (Lampugnani, 1999; Kornyei et al., 2000). A wound was made in astrocyte monolayer grown on plastic dishes, by scraping the bottom of the dish with a sterile 200-μl pipette tip. At the same time point, 1 mM ATP was applied to the cultures, which were maintained in normal growth medium. Five to eight random fields per each dish, in six independent culture preparations, were captured at 0 hr time on a Carl Zeiss AxioObserver A1 inverted microscope (A-Plan 10× objective) by

EM512 CCD Digital Camera System (Evolve, Photometrics). Consecutive images of selected microscopic fields were then captured every 2 hr and stored as digitalized data. From stored images, relative wound area and wound width (μm) was determined using the ImageJ software package. Wound closure, as a result of astrocytic process elongation and cell migration, under the control and treatment conditions, was assessed by calculating the ratio between the wound area at a defined time point and the initial wound area at 0 hr. Data are expressed as mean relative closed area (± SEM) from $n = 6$ separate culture preparations.

Wounded cultures (control and treated with ATP) were grown on glass coverslips (25 mm), prefixed in 4% PFA after 24 hr, and subjected to immunofluorescence labeling for GFAP and DAPI. Images of microscopic fields along the scratch wound were captured with the confocal laser scanning microscope (LSM 510, Carl Zeiss GmbH, Jena, Germany) using Ar Multi-line (457, 478, 488, and 514 nm) laser and Plan-Neofluar 20× objective.

Enzyme-Linked Immunosorbent Assay

Quantitative IL-1β measurements were performed in cell-free supernatants collected at different time points after ATP addition (15 min to 24 hr), using the ELISA and the exact protocol described by the manufacturer. The culture medium was removed at the indicated time after addition of ATP (5 μM to 1 mM) and centrifuged 10 min at 500*g* (Beckman TA-10) to pellet residual cells. Supernatants were carefully removed and used for IL-1β measurements. Colorimetric reactions were quantified on a microplate reader (LKB 5060-006, Micro Plate Reader, Vienna, Austria) at 405 nm, with wavelength correction at 650 nm. Measurements were performed in triplicate, in three independent culture preparations, and data were expressed as mean nanograms per milliliter (± SD). Media obtained from astrocytes treated with LPS (1 μg/ml), alone or in a combination with IFN-γ (100 U/ml) or ATP (1 mM), were used as a positive control.

Western Blot Analysis

Astrocytes (2×10^4 cells/cm^2) were seeded on 10-cm-diameter Petri dishes for purposes of total protein isolation or medium collection. For the total protein isolation, after the treatment, cells from different dishes were collected into separate tubes, centrifuged for 5 min at 500*g*, and resuspended in 500 μl of cold RIPA lysis buffer supplemented with 0.5% w/v protease inhibitor cocktail. The suspensions were kept on ice for 30 min and subsequently centrifuged at 10,000*g* for 10 min, at 4°C (Beckman, JA-20). The supernatant was carefully separated from the pellet, and the protein concentration was determined using the BCA protein assay kit, according to the manufacturer's instruction. Total proteins were used for GFAP/actin analysis. For the culture medium preparation, astrocytes were treated with 1 mM ATP or 1.25 mM probenecid alone or for 30 min pretreatment. Culture medium was removed at the indicated time and centrifuged for 10 min at 500*g* (Beckman, TA-10) to pellet residual cells. The supernatant left after the centrifugation was carefully removed and used for Western blot analysis of released IL-1β.

Culture medium samples were diluted in the sample buffer (375 mM Tris-HCl, pH 6.8, 12% sodium dodecyl sulfate [SDS], 60% [w/v] glycerol, 0.03% bromophenol blue) at a 5:1 volume ratio, and resolved on 12% SDS-PAGE gels. For positive control, the recombinant rat IL-1β/IL-1F2 was used (200 ng/ml, R&D Systems, Minneapolis, MN). Proteins were transferred to a PVDF support membrane and blocked with 5% BSA in Tris buffer saline/Tween 20 (TBST). The overnight blot incubation with polyclonal goat anti-rat IL-1β biotinylated antibody, polyclonal rabbit anti-rat GFAP, or monoclonal mouse anti-rat β-actin, at 4°C, was followed by 2-hr incubation with the avidin-horseradish peroxidase conjugate for the goat anti-rat IL-1β, and donkey anti-rabbit-HRP or donkey anti-mouse-HRP secondary antibodies for GFAP and β-actin, respectively (1:1,000 in PBS, at RT). After intense membrane washing with TBST, the visualization was conducted with the use of chemiluminescence and X-ray films (Kodak, Rochester, NY).

Superoxide Anion Radical Determination

The content of superoxide anion radical ($O_2^-\cdot$) was quantified by the method based on the reduction of nitroblue tetrazolium to monoformazan by $O_2^-\cdot$ in the alkaline nitrogen-saturated medium. The yellow color of the reduced product was measured spectrophotometrically at 550 nm (Auclair and Voisin, 1985). Results are expressed as mean $O_2^-\cdot$ concentration (μmol/l) ± SEM from three independent determinations performed in duplicate.

Nitric Oxide Determination

Astrocytes (2×10^4 cells/cm^2) were plated and treated as described. After the indicated time, supernatants were prepared from culture media, and cells were collected and lysed for nitric oxide (NO) determination. NO was determined spectrophotometrically at 492 nm, by measuring nitrite concentration using the colorimetric method of Griess, after transforming nitrates into nitrites by cadmium reduction (Navarro-Gonzálvez et al., 1998). Results are expressed as mean NO concentration (μmol/l) ± SEM from three independent determinations performed in duplicate.

Malondialdehyde Determination

Malondialdehyde (MDA) was determined by the spectrophotometric method of Villacara et al. (1989). MDA, a secondary product of lipid peroxidation, gives a red-colored pigment after incubation with thiobarbituric acid (TBA) reagent (15% trichloroacetic acid and 0.375% TBA, water solution, at pH 3.5), at 95°C. Absorbance was measured at 532 nm. Results are expressed as mean MDA concentration (nmol/l) ± SEM from three independent determinations performed in duplicate.

SOD Assay

SOD activity, which combines the activity of two enzyme isoforms, cytosolic Cu/ZnSOD and mitochondrial MnSOD, was evaluated using the epinephrine method. The assay is based on the spectrophotometric determination of a decrease in spontaneous epinephrine auto-oxidation, at

480 nm. The rate of the enzyme activity was followed in a carbonate buffer (50 mM, pH 10.2, containing 0.1 mM EDTA), after the addition of 10 mM epinephrine and 5 mM KCN for MnSOD (Sun and Zigman, 1978). Results are expressed as units per milligram of protein ± SEM, whereas the unit is defined as an amount of protein (enzyme) required for 50% of auto-oxidation of epinephrine, from three independent determinations performed in duplicate.

GSH Content Determination

Astrocytes (2×10^4 cells/dish) were plated and treated as described. After the indicated time, supernatants were prepared from a culture media, and cells were collected and lysed for GSH determination. Total GSH content was determined by DTNB-GSSG reductase recycling assay (Anderson, 1986). The rate of 5-thio-2-nitrobenzoic acid formation, which is proportional to total GSH content, was determined spectrophotometrically at 412 nm. Results are expressed as mean GSH concentration (nmol/l) ± SEM, from three separate determinations performed in duplicate.

Data Analysis

Effects of various ATP concentrations on cell proliferation, morphological alterations, IL-1β release, SOD, NO, and GSH levels were analyzed by comparing the means (absolute values) by one-way ANOVA, followed by Tukey post hoc test, with a significance level of $P < 0.05$. The migratory capacities of astrocytes under control and 1 mM ATP treatment conditions were determined by quantifying the ratio between wound area at defined time points and initial wound area (0 hr). Data were compared by Student *t*-test for paired data, at significance level of $P < 0.05$. All statistical analyses were performed using the Origin 7.0 software package.

RESULTS

Extracellular ATP Increases Proliferation of Cortical Astrocytes In Vitro

To assess the effect on cell viability, cells were exposed to ATP (5 μM to 1 mM) for 24 hr and subjected to MTT assay and Annexin V/PI staining. ATP increased formazan absorbance with the concentration (Fig. 1A), with values being significantly different compared with control ($P < 0.05$), except for 5 μM ATP. The nucleotide, however, did not alter the cells' status—that is, the percentages of viable, apoptotic, and necrotic cells remained the same (Table II). Since ATP did not induce apparent cytotoxic effects, double Ki-67/DAPI fluorescence staining was performed to evaluate the effect of ATP on astrocyte proliferation (Fig. 1B, D). While the cells in the control culture proliferated at ~15% rate, in cultures treated with ATP, the proliferative rate increased up to 40% ($F[4,44] = 34.99$, $P < 0.01$), except for cultures treated with the lowest ATP concentration. The maximum proliferative effect was observed in the presence of 1 mM ATP, which induced sustained increase ($P < 0.05$) in the proliferation rate even after 48 hr in culture ($F[2,22] = 63.59$, $P < 0.001$) (Fig. 1C).

Extracellular ATP Induces Shape Remodeling and Reorganization of Astrocyte Filament Networks

Since activation of astrocytes involves distinct changes in cell morphology, we next assessed the effect of ATP on astrocyte shape remodeling. Images of the microscopic fields were captured every 2 hr after ATP treatment (Fig. 2). Although the cells in the control culture were heterogeneous in morphology, the majority of cells displayed enlarged polygonal cell bodies without processes (Fig. 2A). Following addition of ATP, cells developed spherical cell bodies and stellate morphology, with multiple finely branched processes. Shape remodeling was observed even 2 hr after the treatment and appeared stable over time given that the cells did not revert to their previous morphology after 24 hr.

Observed morphological alterations were quantified in terms of changes in cell body area and percentage of cells displaying process-bearing morphology (arbitrarily defined as three or more processes per cell). All ATP concentrations induced a similar decrease in mean cell body area in comparison with control (Fig. 2B). The effect was evidenced 2 hr after ATP treatment ($P < 0.001$) and appeared stable for at least 24 hr ($P < 0.05$). The effect of ATP on stellation appeared to be dose-dependent, with the maximum effect observed with 1 mM ATP treatment. An increase in the percentage of cells bearing processes (Fig. 2C) was observed already after 2 hr ($F[3,20] = 27.58$, $P < 0.001$) and peaked 6 hr after exposure to ATP ($F[3,20] = 237.6$, $P < 0.001$). Twenty-four hours after the treatment, the vast majority of cells treated with 10 μM ATP reverted to their earlier morphology, whereas the changes induced with the higher ATP concentrations appeared to be more stable (Fig. 2A).

Since the reorganization of the cytoskeletal network precedes morphological alterations induced by external stimuli, we next evaluated the effect of ATP on the microfilament and the intermediate filaments network (Fig. 3). In the control culture, enlarged polygonal cells displayed actin fibers organized in fine hypolemmal bundles and delicate centrifugal meshwork, while GFAP filaments formed an elaborate network extending from the perinuclear region to the cell membrane (Fig. 3A, B). In the culture exposed to 5 μM ATP, cells were less polygonal and actin filaments were seen as slightly more prominent fibers (Fig. 3C, D). However, higher ATP concentrations induced almost complete disappearance of hypolemmal and centrifugal actin filaments and led to the progressive increase in cross-linked stress fibers organized in parallel arrays, together with apparent condensation of GFAP filaments in the perinuclear region (Fig. 3E–I). In highly stellate cells treated with 1 mM ATP, elongated GFAP-containing processes were devoid of stress fibers (Fig. 3J). However, all the aforementioned alterations occurred without apparent changes in the actin and GFAP, at both the mRNA (data not shown) and protein levels (Fig. 3K, L).

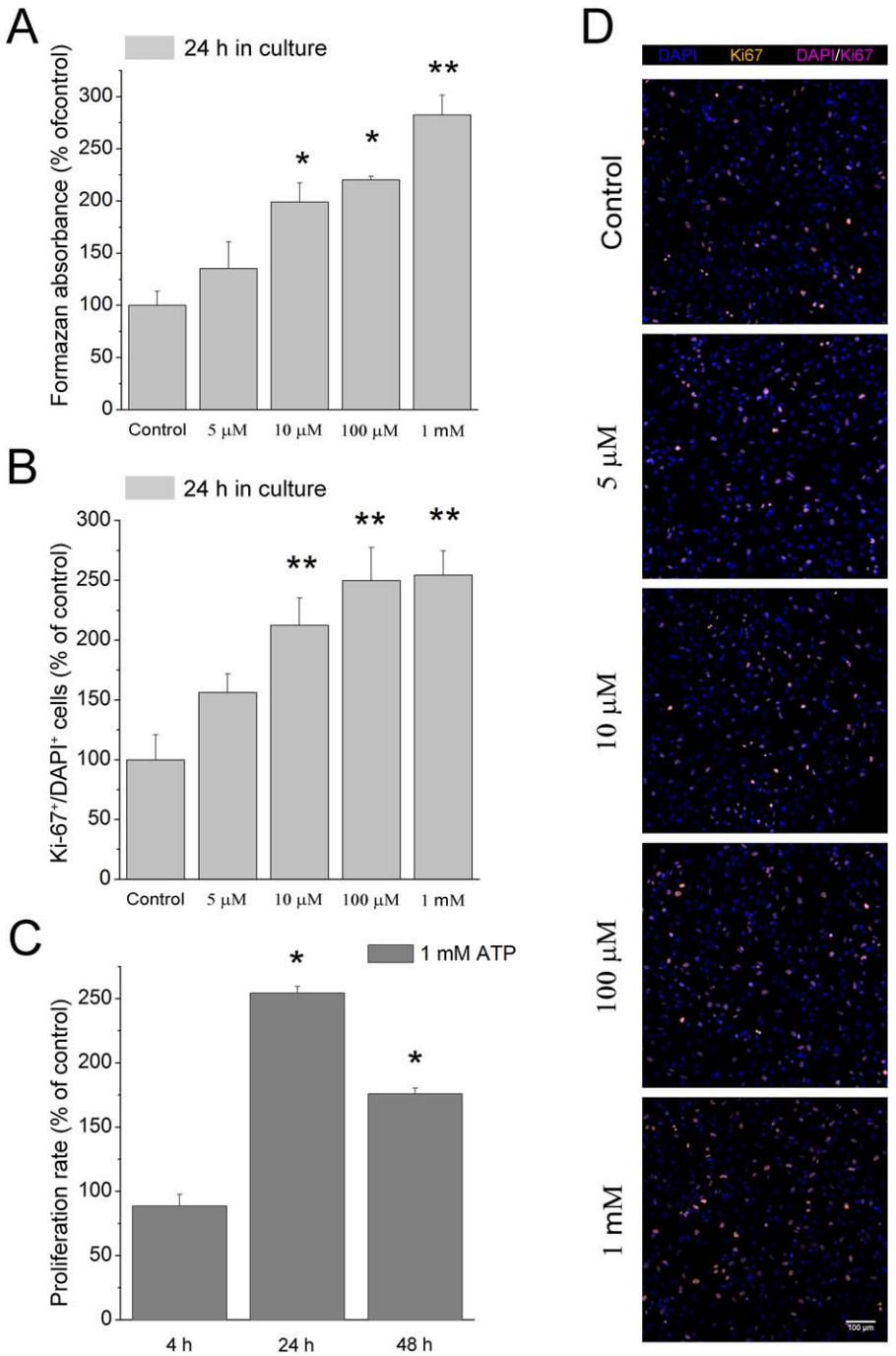

Fig. 1. Effect of ATP on the cell status of cortical astrocyte culture. Cortical astrocytes were treated with ATP (5 μM to 1mM) for 24 hr. **A**: Cell viability was assessed spectrophotometrically by measuring formazan absorbance in MTT test. Bars represent the mean value of formazan absorbance (percentage of control) ± SEM, from three separate culture preparations with three replicates per concentration. **B**: The proliferation of astrocytes in the culture was determined by double Ki-67/DAPI fluorescence labeling, after treating the cells with the indicated ATP concentration for 24 hr. The number of proliferating cells out of the total number of cells in the same field ($Ki\text{-}67^{+}/DAPI^{+}$) was counted from six to eight fields per each coverslip using ImageJ. Bars present mean percentage of proliferating cells (± SEM), from two independent culture preparations. **C**: The proliferation rate of cells treated with 1 mM ATP over time in culture (4–48 hr). Level of significance shown inside the graph: $\star P < 0.01$; $\star\star P < 0.001$. **D**: Representative images of Ki-67/DAPI staining. The cultures were fixed 24 hr after treatment with different ATP concentrations (5 μM to 1mM). Scale bar: 100 μm. [Color figure can be viewed at wileyonlinelibrary.com]

TABLE II. Flow Cytometry Quantification of Cell Survival

ATP treatment	0 (control)	5 μM	10 μM	100μM	1 mM
4 hr treatment	Cell population (%)				
Annexine V^-/PI^-	92.29	93.33	92.82	92.34	90.52
Annexine V^+/PI^-	0.16	0.16	0.17	0.18	0.18
Annexine V^-/PI^+	0.57	0.82	0.62	0.85	0.71
Annexine V^+/PI^+	6.98	5.7	6.39	6.63	8.59
24 hr treatment	Cell population (%)				
Annexine V^-/PI^-	92.29	93.64	95.46	95.58	94.60
Annexine V^+/PI^-	0.16	0.10	0.19	0.16	0.14
Annexine V^-/PI^+	0.57	0.43	0.31	0.31	0.49
Annexine V^+/PI^+	6.98	5.82	4.04	3.94	4.77

ATP Does Not Affect Astrocyte Migration in the Wound-Healing Assay

One of the hallmarks of the reactive phenotype of astrocytes in vivo is their ability to migrate, which results in the formation of a glial scar. Therefore, the ability of ATP to promote migration of astrocytes was analyzed using the in vitro wound-healing assay (Fig. 4A). In both control and ATP-treated cultures, dynamics of wound healing were inversely proportional to the initial wound width (Fig. 4B, C). In scratches with initial wound width of < 300 μm, approximately 4 hr elapsed before detectable front displacement could be observed, whereas after 24 hr

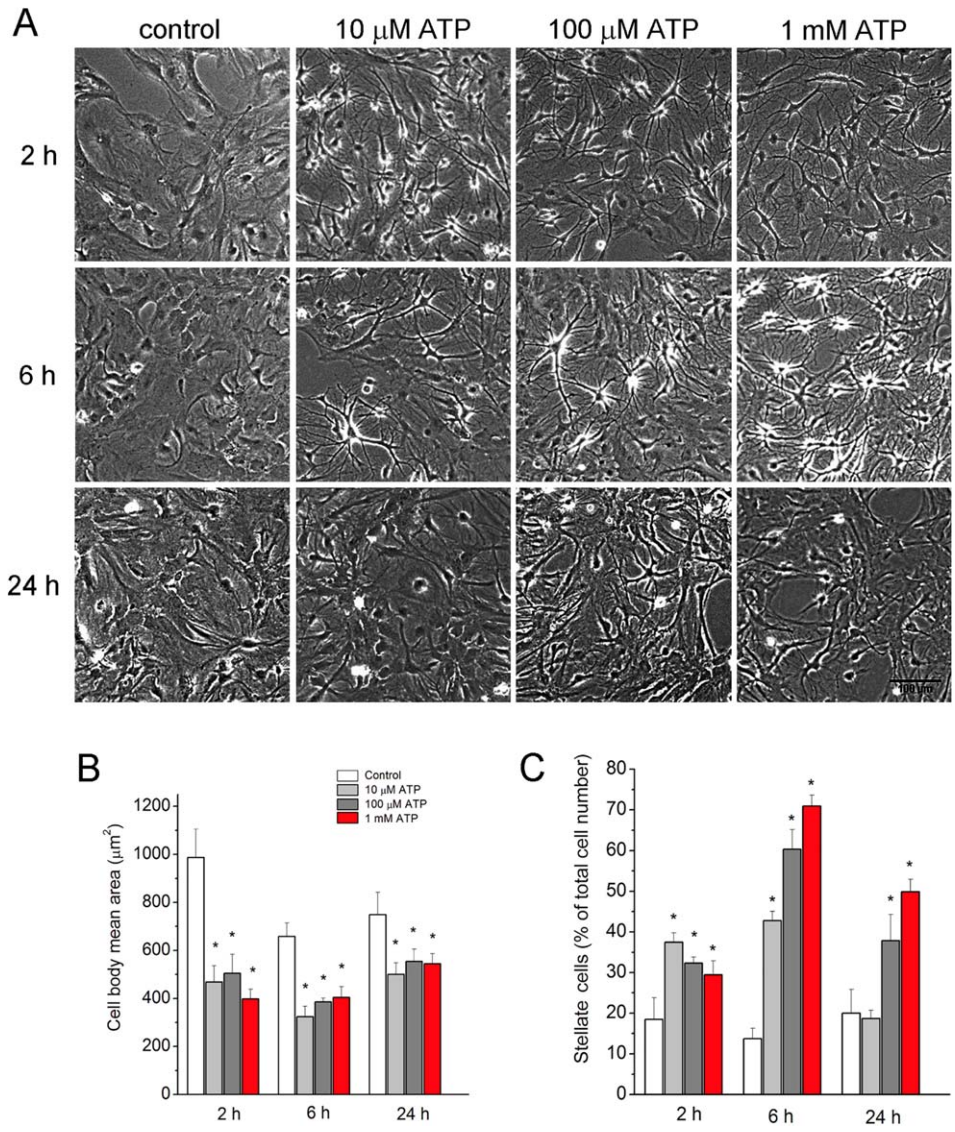

Fig. 2. Effect of ATP on cell morphology. Cell morphology was analyzed after the addition of ATP (10 μM to 1 mM). **A**: Cells from at least six fields per each culture dish were captured on an AxioObserver A1 inverted microscope in two independent experiments, encompassing six randomly chosen fields in each group, and representative micrographs captured at 2, 6, and 24 hr after treatment are presented. Scale bar: 100 μm. **B**: Mean cell body area was analyzed using the ImageJ software package, and the results are presented as mean cell body area (μm^2) ± SEM. **C**: The number of stellate cells (defined as more than three primary processes per cell) was counted using the ImageJ software package and expressed as a percentage out of a total number of cells in culture (± SEM). Level of significance indicated in the graphs: $\star P < 0.01$. [Color figure can be viewed at wileyonlinelibrary.com]

the wounds were almost completely closed in both control and ATP-treated cultures (Fig. 4A). However, in scratches where the initial wound width was > 300 μm, dynamics of wound healing markedly slowed down, leaving the wound area uncovered even after 48 hr (Fig. 4B). Since the dynamics of wound healing critically depend on initial wound width, this finding indicates the involvement of a diffusible factor(s) in the process. To dissect the effect of ATP in this matter, relative wound closure was quantified in control and ATP-treated cultures with initial wound width of 250 to 350 μm (Fig. 4C). The results demonstrated that addition of ATP did not alter the process of wound healing, at either time point ($P > 0.05$), but it did alter the appearance of the cells at the wound edge (Fig. 5), in a similar way as demonstrated in nonwounded cultures (Fig. 2). Specifically, in nontreated cultures, cells at the wound edge developed radially oriented short hypertrophic processes, while in cultures treated with ATP, cells developed elongated processes directed toward the denuded area (Fig. 5).

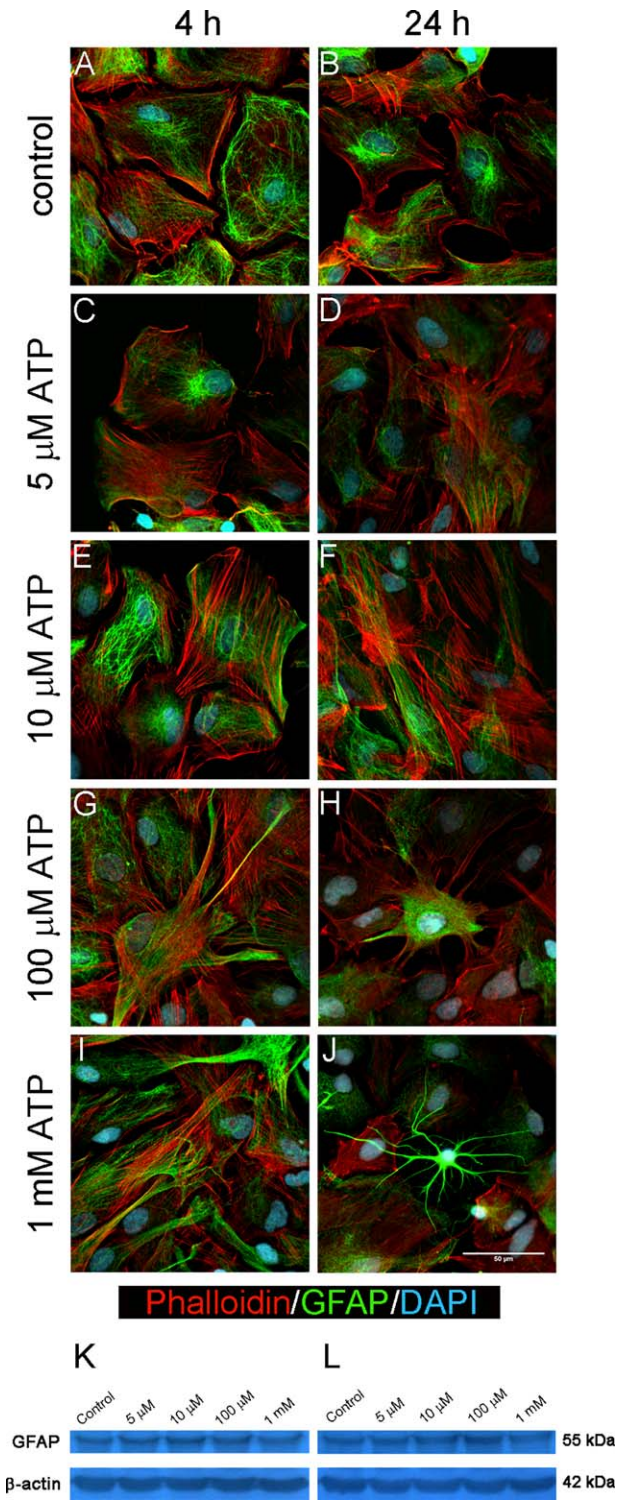

Fig. 3. Effect of ATP on cytoskeletal network in astrocytes. Organization of microfilaments and intermediate filaments in primary cortical astrocytes treated with ATP was determined by double immunofluorescence labeling of actin (*red*) and GFAP (*green*). Cell nuclei were counterstained with DAPI (*blue*). Images of nontreated astrocytes (**A, B**) show cells with a polygonal shape, with actin bundles lining the cell edges. ATP treatment induced increased presence of stress fibers organized in parallel arrays, 4 and 24 hr after the treatment (**C–J**). Stellation led to significant reorganization of cytoskeleton at 100 μM ATP (**H**) and 1 mM ATP (**J**). Scale bar: 50 μm. Western blot did not show the total GFAP or actin change in the cultures 4 hr (**K**) or 24 hr (**L**) after ATP treatment. [Color figure can be viewed at wileyonlinelibrary.com]

Extracellular ATP Alone Does Not Induce IL-1β Release by Cortical Astrocytes

Given that induction of reactive phenotype in astrocytes critically depends on IL-1β, we next investigated whether ATP evokes cytokine release from cultured astrocytes. Cultures were treated with ATP (5 μM to 1 mM), and the levels of IL-1β were determined in the culture medium, 15 min to 24 hr after addition of ATP. Separate astrocyte cultures were treated with LPS alone, LPS +IFNγ, and LPS +IFNγ+ ATP and the culture media 24 hr after the treatments were used for IL-1β determination. While LPS and LPS + IFNγ evoked significant IL-1β release by cultured astrocytes (Fig. 6A), regardless of the concentration and sampling time point after treatment, ATP did not change the cytokine level in the culture medium, which is in line with studies on immune cells (Ferrari et al., 1997). Moreover, ATP did not add to the IL-1β release by cells primed with LPS + IFNγ. The absence of IL-1β release following ATP treatment was confirmed by Western blot analysis (Fig. 6B).

Extracellular ATP Enhances Antioxidative Systems in Cortical Astrocytes

Oxidative stress is defined as a significant increase in production of ROS and RNS, such as $O_2^-\cdot$ and NO. These two molecular species react readily to produce peroxynitrite, which further reacts with various cellular components. MDA is the end product formed by degradation of cell membrane phospholipids and is usually used as an index of lipid peroxidation. In the next set of probes, we

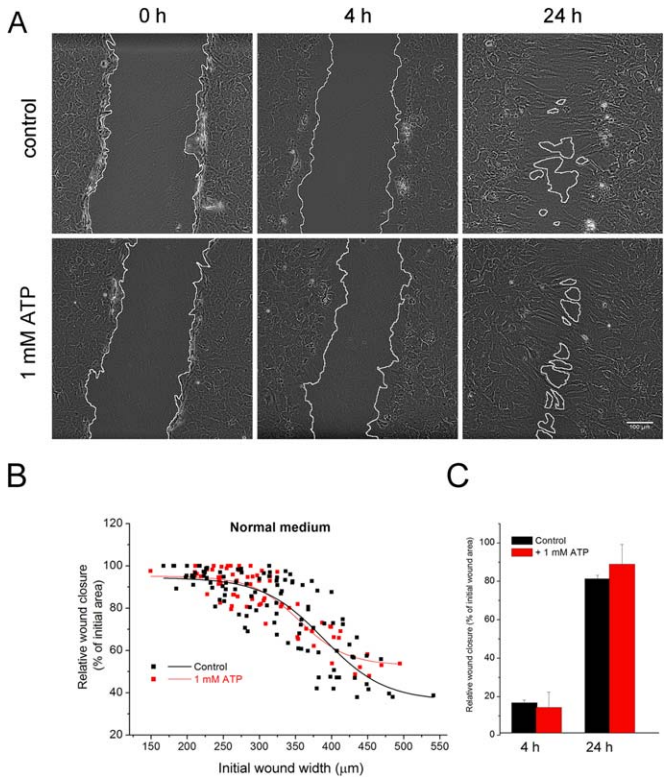

Fig. 4. Effect of ATP on astrocyte migration in wound-healing assay. Astrocytes were grown to confluence in normal medium, and a wound was made by scraping the bottom of the dish with a sterile 200-μl pipette tip. **A**: 1 mM ATP was applied, and healing of denuded area was analyzed under the microscope every 2 hr. Representative micrographs after 4 and 24 hr are presented. Wound edges were provisionally marked in white. Scale bar: 100 μm. **B**: Wound area, measured using the ImageJ software package at different time points, is expressed relative to the initial wound area (at 0 hr). The graph represents relative closure of wound areas in control (*black*) and ATP-treated cultures (*red*), as a function of initial wound width (μm), indicating that dynamics of wound healing depend on initial wound width and are not altered by the addition of ATP. **C**: Relative wound closure (± SEM) in control (*black bar*) and ATP-treated cultures (*red bars*), at 4 and 24 hr in cultures with initial wound area of 250 to 350 μm. [Color figure can be viewed at wileyonlinelibrary.com]

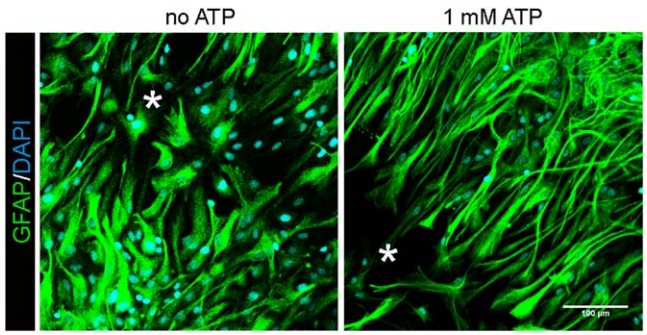

Fig. 5. Effect of ATP on morphology of astrocytes at the wound edge. Cultures were grown and treated as described. Images show GFAP immunofluorescence of cells at wound edges. Cells not treated with ATP developed short, radially extending hypertrophic processes, whereas cells treated with ATP developed long and narrow processes extending in parallel toward the denuded area. White star marks the wound area. Scale bar: 100 μm. [Color figure can be viewed at wileyonlinelibrary.com]

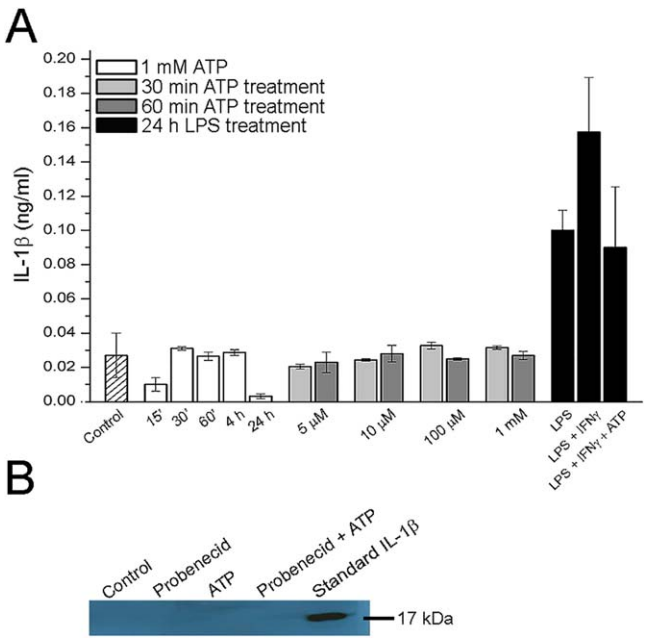

Fig. 6. Effect of ATP on IL-1β release by cultured astrocytes. **A**: Astrocytes were treated with 1 mM ATP for the indicated period of time (*white bars*) or with increasing concentrations of ATP for 30 min (*light gray bars*) or 60 min (*gray bars*). Levels of IL-1β in cell-free culture media were determined by ELISA. The cell-free culture media of astrocytes treated with LPS, LPS+IFN-γ, or LPS+IFN-γ+ATP were used as a positive control (*black bars*). Bars present mean IL-1β (ng/ml) from three independent determinations performed in triplicate (± SEM). **B**: Western blot analysis of cell-free culture media obtained from control culture and cultures treated with 1 mM ATP, 1.25 mM probenecid, or combined. Probenecid was applied as pannexin hemichannel blocker. The recombinant rat IL-1β/IL-1F2 was used as standard IL-1β (positive control). [Color figure can be viewed at wileyonlinelibrary.com]

evaluated the potency of ATP to induce oxidative stress in cultured astrocytes, by determining the levels of $O_2^-\cdot$, NO, and MDA in the cells 4 and 24 hr after treatment (Fig. 7). The levels of $O_2^-\cdot$, NO, and MDA under control conditions did not vary over time or after ATP treatment (Fig. 7A–C). However, ATP induced a dose-dependent increase in Cu/ZnSOD ($P < 0.01$) and MnSOD ($P < 0.05$) activity (Fig. 7D, E), together with a marked increase in intracellular ($P < 0.001$) and extracellular ($P < 0.001$) GSH content (Fig. 7F, G).

DISCUSSION

It is widely accepted that extracellular ATP acts as a danger-associated molecular pattern in all tissues, including the brain, where it induces inflammatory responses of

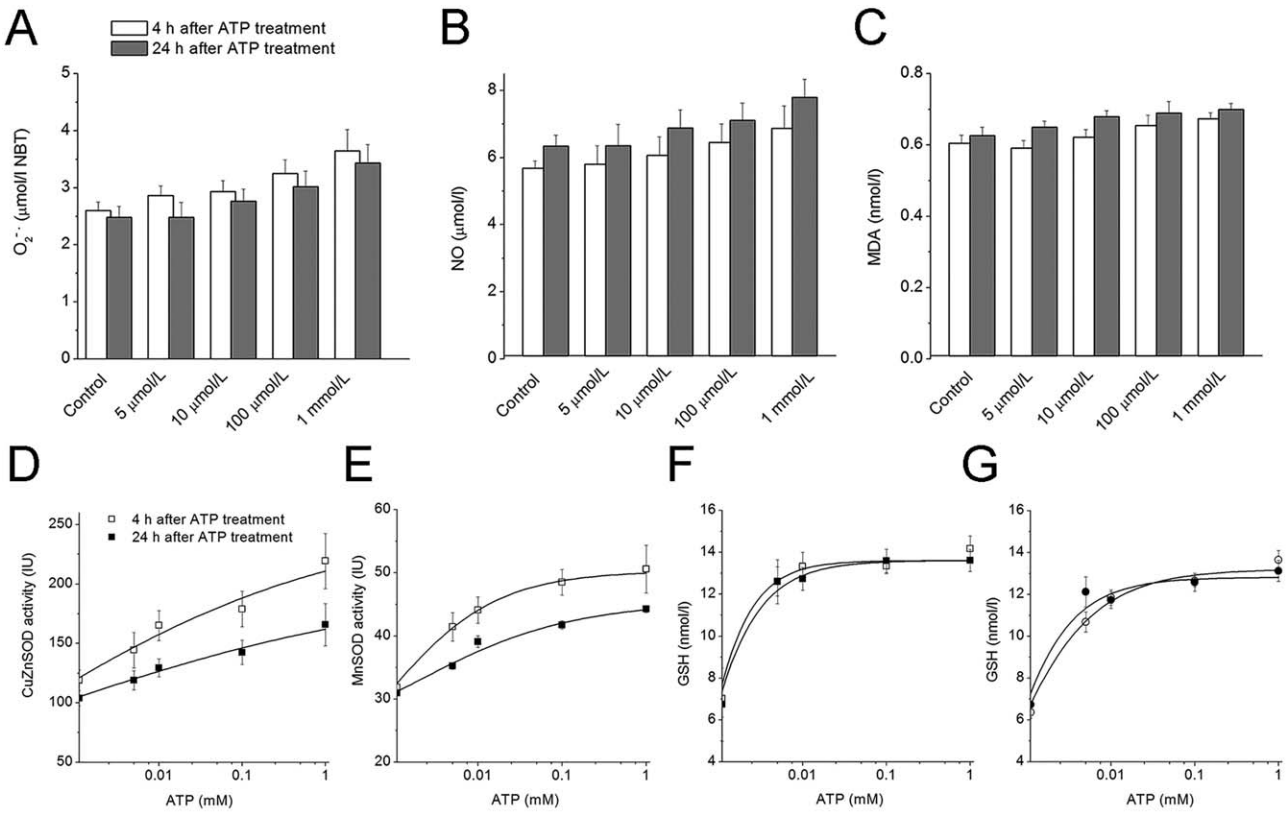

Fig. 7. Effect of ATP on oxidative status and antioxidative defense of the cultured astrocyte. Levels of (**A**) $O_2^{-}\cdot$, (**B**) NO, and (**C**) MDA in whole-cell lysates obtained from control cultures and cultures treated with ATP for 4 hr (*light gray*) and 24 hr (*dark gray*) after addition of ATP. Bars present mean (± SEM) from three separate culture preparations, performed in duplicate. Effect of ATP on (**D**) Cu/ZnSOD and (**E**) MnSOD activities in the whole-cell lysates, and GSH content in lysates (**F**) and in (**G**) cell-free culture media obtained from control cultures and cultures treated with ATP at 4 hr (*open symbol*) and 24 hr (*black symbol*) after the addition of ATP. Symbols represent mean ± SEM from three separate determinations, performed in duplicate.

microglia and astrocytes after any type of brain insult. However, results of the current study demonstrate that although ATP triggers several attributes of activated astrocytic phenotype, at a magnitude that increases with concentration, it is not sufficient to induce full-blown reactive phenotype of astrocytes. Therefore, our results suggest that the effects of extracellular ATP in the brain in vivo may be both inflammatory and protective/adaptive, depending not just on its local concentration but also on the presence of co-acting factors and downstream events in the exact tissue context.

The responses of cultured astrocytes in terms of their proliferation rate and cell shape remodeling reflect activation effects of ATP. Specifically, astrocytes grown in culture displayed enlarged polygonal shape, with actin bundles lining the cell edges. As a result of cell body enlargement after some time in culture, the cells gradually decrease their proliferation rate and begin to senesce (Lewis et al., 2008). Therefore, the proliferation of astrocytes after exposure to a noxious stimulus reflects their activation, both in vitro (Gallo et al., 2000) and in vivo (Sofroniew, 2009). While it is known that ATP exerts a mitogenic effect on astrocytes in vivo (Franke et al., 2006), the effects in vitro depend on ATP concentration, duration of treatment, cell density, and purity of the culture itself (Ciccarelli et al., 1994; Neary et al., 1994, 1999; Quintas et al., 2011). In our culture system, 5 μM ATP did not induce proliferation, morphological changes, or underlying reorganization of cytoskeletal elements, while higher concentrations promoted cell proliferation in a dose- and time-dependent manner. In addition, ATP induced cell shape remodeling. Particularly, resting cells with a polygonal shape condensed their cell bodies and developed fine processes following exposure to ATP. While cell body size decreases were comparable for all ATP concentrations applied, the proportion of cells that displayed stellate morphology increased with ATP concentration. The process-bearing morphology represents the typical appearance of reactive astrocytes in vivo (Franke et al., 2012) and the feature of their reactive phenotype in vitro (Renner et al., 2013). In that manner, stellation of astrocytes in culture, which may be induced by several noxious stimuli, including pH alterations, amyloid-β, TNF-α, and brain extracts in serum-free medium (Favero and Mandell, 2007), requires the reorganization of the cytoskeleton (John et al., 2004). In our

system, ATP-induced stellation was accompanied by conversion of actin fibers into a robust network of stress fibers running below the plasma membrane and bundling of the intermediate filaments along progressively longer processes. However, the cytoskeleton rearrangements occurred without upregulation of GFAP, which is the hallmark of a fully developed astrogliotic phenotype.

Given that formation of stress fibers is crucial for force generation during the cell migration (Parsons et al., 2000; John et al., 2004), it has been of interest to test whether ATP promotes this aspect of the reactive phenotype in astrocytes. ATP did not alter cell migration or dynamics of wound healing, although it induced reorganization of the cytoskeleton and elongation of the processes at the wound edge. Moreover, ATP alone was not sufficient to induce IL-1β release by cultured astrocyte, and it did not potentiate the cytokine release from LPS+IFNγ–primed astrocytes, as it did from the microglial cells (Ferrari et al., 1997). Above all, our results demonstrate that ATP does not induce oxidative damage in astrocytes, but instead strengthens their antioxidative defense, by stimulating SOD activities and by increasing their intracellular GSH content and extracellular release. In neurons, which have intense metabolism and massive production of the peroxide, the role of astrocytes against the toxicity appears to be particularly important (Dringen et al., 2000).

Although we did not experimentally address this question, both nucleotide-sensitive P2 receptors and adenosine-sensitive P1 purinoreceptors may be responsible for the observed responses of astrocytes. P2 receptors differ in their affinity for ATP and ADP; hence, the observed responses of cultured astrocytes to the range of applied ATP concentrations may be mediated via a subset of P2X and P2Y purinoreceptors (Burnstock and Knight, 2004; Abbracchio et al., 2006). Namely, a particular heteromeric and/or homomeric combination of P2X1-7 subunits forms a functional channel with a distinct affinity for ATP and desensitization dynamics (North, 2002), while among P2Y receptors, $P2Y_2$, $P2Y_4$, and $P2Y_{11}$ may be directly activated by ATP. Therefore, the effects of extracellular ATP will depend on specific composition and localization of purinoreceptors at primary cortical astrocytes (Coddou et al., 2011). Astrocytes are shown to express a subset of P2X and P2Y receptors, whereas different combinations were demonstrated in vivo and in culture conditions at different developmental stages (Quintas et al., 2011). Primary cortical astrocyte cultures obtained from 1-day-old rat pups express $P2Y_1$, $P2Y_2$, and $P2Y_4$ (Lenz et al., 2000) and P2X1-7 receptor subtypes (Jacques-Silva et al., 2004). Therefore, it is likely that ATP, in the concentration range applied, activates a combination of P2X1-7, $P2Y_2$, and $P2Y_4$ receptors with the overlapping affinities towards ATP. Moreover, cultured astrocytes express the enzyme chain for extracellular ATP hydrolysis, with the highest relative abundance of NTPDase2 and ecto-5'-nucleotidase (Brisevac et al., 2015), which produce ADP and adenosine, respectively. Therefore, besides the direct effects mediated by ATP-sensitive $P2Y_2$ and $P2Y_4$ receptors, some of the observed effects may be mediated via ADP-sensitive $P2Y_1$ and a subset of adenosine-sensitive P1 receptors expressed on astrocytes in vitro (Boison 2012; Chen et al., 2014). Results from agonist and antagonist binding studies on cultured systems indicate involvement of P2X2 and $P2Y_1$ receptors in ATP-induced proliferation and IL-1β release by astrocytes, both in vitro (Neary et al., 1994, 1999, 2003; Xia and Zhu, 2011) and in vivo (Franke et al., 1999, 2001), while a decrease in NO production by downregulating NOSII expression may be induced by P2Y1 antagonists, such as suramin and oATP (Liu et al., 2000). On the other hand, some of the effects may be induced by adenosine, which is an important modulator of astrocyte function in emergency situations, when it resets the cell energy balance and protects astrocytes from ischemic damage (Boison, 2012). It should be noted, however, that the responses of astrocytes may differ in vivo, depending on a distinct combination of purinoreceptors, pannexin hemichannels, nucleoside transporters, and purine-converting enzymes present in the particular tissue context. Moreover, observed ATP-induced responses of astrocytes in culture may not completely replicate the behavior of astrocytes integrated into the brain parenchyma, since the cells, as the main sensors of neuronal homeostasis, adapt to neuronal functioning by expressing receptors for nearly all signals produced by neurons. Therefore, the responses of astrocytes induced by an initial stimulus, like ATP, dynamically change, both temporally and spatially, with later molecular signals produced by neurons in a particular tissue environment. In conclusion, extracellular ATP activates cultured astrocytes in several respects, although it is not able to evoke their full-blown reactive phenotype in vitro. According to recently the formulated two-hit hypothesis for neuroinflammation (Fiebich et al., 2014), upon damage all vertebrate cells release large amounts of ATP into the extracellular space. The first hit, the injury itself, leads to release of the large pools of cytosolic ATP into the extracellular milieu. Liberated ATP acts at purinergic receptors, inducing the effects that crucially depend on the nature of two downstream factors: the type of receptors present on cells within the vicinity of the injury, and the distribution and activity of hydrolyzing ectonucleotidases. Therefore, extracellular ATP may modulate neuroinflammation by exerting responses of astrocytes, both neuroinflammatory and adaptive, which depend on exact tissue context, other cellular targets, local concentration, and prevailing extracellular environment. Identifying responses of astrocytes to extracellular ATP may help to provide alternative approaches to reduce neuroinflammation associated with all types of neurological disorders.

CONFLICT OF INTEREST

The authors have no conflict of interest to declare.

ROLE OF AUTHORS

All authors contributed sufficiently for being listed as authors of this article. Study design: NN and MA. Animal

handling, cell culture preparation and treatment: MA, MM. Immunocytochemistry, actin and GFAP immunolabeling, cell proliferation assay, MTT assay, wound-healing assay, ELISA: MA. Western blot: MA, DL. Flow cytometry: IB, MJ, MA. Morphometric analysis: NN. Determination of superoxide anion radical, nitric oxide, and glutathione: IS, NJ, IL. Superoxide dismutase enzyme assay: IS, NJ, IL. Data analysis and interpretation: NN, MA, DL. Writing of article: NN, MA. Final approval of version to be published: MA, MJ, DL, IB, IMB, IL, IS, NJ, MM.

DATA ACCESSIBILITY

The following tools, software, and databases were used. Image analyses were conducted using *ImageJ* (http://imagej.nih.gov/ij/download.html; RRID:SCR_ 003070). Statistical analysis was performed using the Origin 7.0 software package (http://www.originlab.com/index.aspx?go=PRODUCTS/Origin; RRID:SCR_014212).

REFERENCES

Abbracchio MP, Burnstock G, Boeynaems JM, Barnard EA, Boyer JL, Kennedy C, Knight GE, Fumagalli M, Gachet C, Jacobson KA, et al. 2006. International Union of Pharmacology LVIII: update on the P2Y G protein-coupled nucleotide receptors: from molecular mechanisms and pathophysiology to therapy. Pharmacol Rev 58:281–341.

Anderson ME. 1986. Tissue gluthatione. Boca Raton (FL): CRC Press.

Auclair C, Voisin E. 1985. Nitroblue tetrazolium reduction. Boca Raton (FL): CRC Press.

Bennett MV, Garre JM, Orellana JA, Bukauskas FF, Nedergaard M, Saez JC. 2012. Connexin and pannexin hemichannels in inflammatory responses of glia and neurons. Brain Res 1487:3–15.

Bodin P, Burnstock G. 2001. Purinergic signalling: ATP release. Neurochem Res 26:959–969.

Boison D. 2012. Adenosine dysfunction in epilepsy. Glia 60:1234–1243.

Bours MJ, Swennen EL, Di Virgilio F, Cronstein BN, Dagnelie PC. 2006. Adenosine 5'-triphosphate and adenosine as endogenous signaling molecules in immunity and inflammation. Pharmacol Ther 112:358–404.

Bours MJ, Dagnelie PC, Giuliani AL, Wesselius A, Di Virgilio F. 2011. P2 receptors and extracellular ATP: a novel homeostatic pathway in inflammation. Front Biosci 3:1443–1456.

Brisevac D, Adzic M, Laketa D, Parabucki A, Milosevic M, Lavrnja I, Bjelobaba I, Sevigny J, Kipp M, Nedeljkovic N. 2015. Extracellular ATP selectively upregulates ecto-nucleoside triphosphate diphosphohydrolase 2 and ecto-5'-nucleotidase by rat cortical astrocytes in vitro. J Mol Neurosci 57:452–462.

Burnstock G, Knight GE. 2004. Cellular distribution and functions of P2 receptor subtypes in different systems. Int Rev Cytol 240:31–304.

Burnstock G, Fredholm BB, Verkhratsky A. 2011. Adenosine and ATP receptors in the brain. Curr Top Med Chem 11:973–1011.

Cahill CM, Rogers JT. 2008. Interleukin (IL) 1beta induction of IL-6 is mediated by a novel phosphatidylinositol 3-kinase-dependent AKT/IkappaB kinase alpha pathway targeting activator protein-1. J Biol Chem 283:25900–25912.

Chen JF, Lee CF, Chern Y. 2014. Adenosine receptor neurobiology: overview. Int Rev Neurobiol 119:1–49.

Ciccarelli R, Di Iorio P, Ballerini P, Ambrosini G, Giuliani P, Tiboni GM, Caciagli F. 1994. Effects of exogenous ATP and related analogues on the proliferation rate of dissociated primary cultures of rat astrocytes. J Neurosci Res 39:556–566.

Coddou C, Yan Z, Obsil T, Huidobro-Toro JP, Stojilkovic SS. 2011. Activation and regulation of purinergic P2X receptor channels. Pharmacol Rev 63:641–683.

Davalos D, Grutzendler J, Yang G, Kim JV, Zuo Y, Jung S, Littman DR, Dustin ML, Gan WB. 2005. ATP mediates rapid microglial response to local brain injury in vivo. Nat Neurosci 8:752–758.

Delekate A, Fuchtemeier M, Schumacher T, Ulbrich C, Foddis M, Petzold GC. 2014. Metabotropic P2Y1 receptor signalling mediates astrocytic hyperactivity in vivo in an Alzheimer's disease mouse model. Nat Commun 5:5422.

Dringen R, Gutterer JM, Hirrlinger J. 2000. Glutathione metabolism in brain metabolic interaction between astrocytes and neurons in the defense against reactive oxygen species. Eur J Biochem 267:4912–4916.

Dunn SL, Young EA, Hall MD, McNulty S. 2002. Activation of astrocyte intracellular signaling pathways by interleukin-1 in rat primary striatal cultures. Glia 37:31–42.

Farina C, Aloisi F, Meinl E. 2007. Astrocytes are active players in cerebral innate immunity. Trends Immunol 28:138–145.

Favero CB, Mandell JW. 2007. A pharmacological activator of AMP-activated protein kinase (AMPK) induces astrocyte stellation. Brain Res 1168:1–10.

Ferrari D, Chiozzi P, Falzoni S, Hanau S, Di Virgilio F. 1997. Purinergic modulation of interleukin-1β release from microglial cells stimulated with bacterial endotoxin. J Exp Med 185:579–582.

Fiebich BL, Akter S, Akundi RS. 2014. The two-hit hypothesis for neuroinflammation: role of exogenous ATP in modulating inflammation in the brain. Front Cell Neurosci 8:260.

Fields RD. 2011. Nonsynaptic and nonvesicular ATP release from neurons and relevance to neuron-glia signaling. Sem Cell Dev Biol 22:214–219.

Franke H, Krugel U, Illes P. 1999. P2 receptor-mediated proliferative effects on astrocytes in vivo. Glia 28:190–200.

Franke H, Krugel U, Schmidt R, Grosche J, Reichenbach A, Illes P. 2001. P2 receptor-types involved in astrogliosis in vivo. Br J Pharmacol 134:1180–1189.

Franke H, Grummich B, Hartig W, Grosche J, Regenthal R, Edwards RH, Illes P, Krugel U. 2006. Changes in purinergic signaling after cerebral injury—involvement of glutamatergic mechanisms? Int J Dev Neurosci 24:123–132.

Franke H, Verkhratsky A, Burnstock G, Illes P. 2012. Pathophysiology of astroglial purinergic signalling. Purinergic Signal 8:629–657.

Fredholm BB, IJzerman AP, Jacobson KA, Linden J, Muller CE. 2011. International Union of Basic and Clinical Pharmacology. LXXXI. Nomenclature and classification of adenosine receptors—an update. Pharmacol Rev 63:1–34.

Gallo F, Morale MC, Spina-Purrello V, Tirolo C, Testa N, Farinella Z, Avola R, Beaudet A, Marchetti B. 2000. Basic fibroblast growth factor (bFGF) acts on both neurons and glia to mediate the neurotrophic effects of astrocytes on LHRH neurons in culture. Synapse 36:233–253.

George J, Goncalves FQ, Cristovao G, Rodrigues L, Meyer Fernandes JR, Goncalves T, Cunha RA, Gomes CA. 2015. Different danger signals differently impact on microglial proliferation through alterations of ATP release and extracellular metabolism. Glia 63:1636–1645.

He Y, Jackman NA, Thorn TL, Vought VE, Hewett SJ. 2015. Interleukin-1beta protects astrocytes against oxidant-induced injury via an NF-kappaB-dependent upregulation of glutathione synthesis. Glia 63:1568–1580.

Idzko M, Ferrari D, Eltzschig HK. 2014. Nucleotide signalling during inflammation. Nature 509:310–317.

Imura Y, Morizawa Y, Komatsu R, Shibata K, Shinozaki Y, Kasai H, Moriishi K, Moriyama Y, Koizumi S. 2013. Microglia release ATP by exocytosis. Glia 61:1320–1330.

Jacques-Silva MC, Rodnight R, Lenz G, Liao Z, Kong Q, Tran M, Kang Y, Gonzalez FA, Weisman GA, Neary JT. 2004. P2X7 receptors

stimulate AKT phosphorylation in astrocytes. Br J Pharmacol 141: 1106–1117.

John GR, Chen L, Rivieccio MA, Melendez-Vasquez CV, Hartley A, Brosnan CF. 2004. Interleukin-1beta induces a reactive astroglial phenotype via deactivation of the Rho GTPase-Rock axis. J Neurosci 24: 2837–2845.

Juranyi Z, Sperlagh B, Vizi ES. 1999. Involvement of P2 purinoceptors and the nitric oxide pathway in [3H]purine outflow evoked by short-term hypoxia and hypoglycemia in rat hippocampal slices. Brain Res 823:183–190.

Khakh BS, North RA. 2012. Neuromodulation by extracellular ATP and P2X receptors in the CNS. Neuron 76:51–69.

Kim JH, Min KJ, Seol W, Jou I, Joe EH. 2010. Astrocytes in injury states rapidly produce anti-inflammatory factors and attenuate microglial inflammatory responses. J Neurochem 115:1161–1171.

Kim SY, Moon JH, Lee HG, Kim SU, Lee YB. 2007. ATP released from beta-amyloid-stimulated microglia induces reactive oxygen species production in an autocrine fashion. Exp Mol Med 39:820–827.

Koizumi S. 2010. Synchronization of Ca2+ oscillations: involvement of ATP release in astrocytes. FEBS J 277:286–292.

Koizumi S, Ohsawa K, Inoue K, Kohsaka S. 2013. Purinergic receptors in microglia: functional modal shifts of microglia mediated by P2 and P1 receptors. Glia 61:47–54.

Kornyei Z, Czirok A, Vicsek T, Madarasz E. 2000. Proliferative and migratory responses of astrocytes to in vitro injury. J Neurosci Res 61: 421–429.

Lampugnani MG. 1999. Cell migration into a wounded area in vitro. Methods Mol Biol 96:177–182.

Lenz G, Gottfried C, Luo Z, Avruch J, Rodnight R, Nie WJ, Kang Y, Neary JT. 2000. P(2Y) purinoceptor subtypes recruit different mek activators in astrocytes. Br J Pharmacol 129:927–936.

Lewis DK, Woodin HR, Sohrabji F. 2008. Astrocytes from acyclic female rats exhibit lowered capacity for neuronal differentiation. Aging Cell 7:836–849.

Lipmann F. 1941. Metabolic generation and utilization of phosphate bond energy. Adv Enzymol Relat Subj 1:99–162.

Liu JS, John GR, Sikora A, Lee SC, Brosnan CF. 2000. Modulation of interleukin-1beta and tumor necrosis factor alpha signaling by P2 purinergic receptors in human fetal astrocytes. J Neurosci 20:5292–5299.

Melani A, Turchi D, Vannucchi MG, Cipriani S, Gianfriddo M, Pedata F. 2005. ATP extracellular concentrations are increased in the rat striatum during in vivo ischemia. Neurochem Int 47:442–448.

Navarro-Gonzálvez JA, Garcia-Benayas C, Arenas J. 1998. Semiautomated measurement of nitrate in biological fluids. Clin Chem 44:679–681.

Neary JT, Baker L, Jorgensen SL, Norenberg MD. 1994. Extracellular ATP induces stellation and increases glial fibrillary acidic protein content and DNA synthesis in primary astrocyte cultures. Acta Neuropathol 87:8–13.

Neary JT, Kang Y, Bu Y, Yu E, Akong K, Peters CM. 1999. Mitogenic signaling by ATP/P2Y purinergic receptors in astrocytes: involvement of a calcium-independent protein kinase C, extracellular signal-regulated protein kinase pathway distinct from the phosphatidylinositol-specific phospholipase C/calcium pathway. J Neurosci 19:4211–4220.

Neary JT, Kang Y, Willoughby KA, Ellis EF. 2003. Activation of extracellular signal-regulated kinase by stretch-induced injury in astrocytes involves extracellular ATP and P2 purinergic receptors. J Neurosci 23: 2348–2356.

North RA. 2002. Molecular physiology of P2X receptors. Physiol Rev 82:1013–1067.

Oberheim NA, Tian GF, Han X, Peng W, Takano T, Ransom B, Nedergaard M. 2008. Loss of astrocytic domain organization in the epileptic brain. J Neurosci 28:3264–3276.

Pankratov Y, Lalo U, Verkhratsky A, North RA. 2006. Vesicular release of ATP at central synapses. Pflugers Arch 452:589–597.

Parsons JT, Martin KH, Slack JK, Taylor JM, Weed SA. 2000. Focal adhesion kinase: a regulator of focal adhesion dynamics and cell movement. Oncogene 19:5606–5613.

Quintas C, Fraga S, Goncalves J, Queiroz G. 2011. P2Y receptors on astrocytes and microglia mediate opposite effects in astroglial proliferation. Purinergic Signal 7:251–263.

Renner NA, Sansing HA, Inglis FM, Mehra S, Kaushal D, Lackner AA, Maclean AG. 2013. Transient acidification and subsequent proinflammatory cytokine stimulation of astrocytes induce distinct activation phenotypes. J Cell Physiol 228:1284–1294.

Rodrigues RJ, Tomé AR, Cunha RA. 2015. ATP as a multi-target danger signal in the brain. Front Neurosci 9:148.

Shih AY, Johnson DA, Wong G, Kraft AD, Jiang L, Erb H, Johnson JA, Murphy TH. 2003. Coordinate regulation of glutathione biosynthesis and release by Nrf2-expressing glia potently protects neurons from oxidative stress. J Neurosci 23:3394–3406.

Silverman WR, de Rivero Vaccari JP, Locovei S, Qiu F, Carlsson SK, Scemes E, Keane RW, Dahl G. 2009. The pannexin 1 channel activates the inflammasome in neurons and astrocytes. J Biol Chem 284: 18143–18151.

Sofroniew MV. 2009. Molecular dissection of reactive astrogliosis and glial scar formation. Trends Neurosci 32:638–647.

Steele ML, Fuller S, Maczurek AE, Kersaitis C, Ooi L, Munch G. 2013. Chronic inflammation alters production and release of glutathione and related thiols in human U373 astroglial cells. Cell Mol Neurobiol 33: 19–30.

Sun J-J, Liu Y, Ye Z-R. 2008. Effects of P2Y1 receptor on glial fibrillary acidic protein and glial cell line-derived neurotrophic factor production of astrocytes under ischemic condition and the related signaling pathways. Neurosci Bull 24:231–243.

Sun M, Zigman S. 1978. An improved spectrophotometric assay for superoxide dismutase based on epinephrine autoxidation. Anal Biochem 90:81–89.

Villacara A, Kumami K, Yamamoto T, Mrsulja BB, Spatz M. 1989. Ischemic modification of cerebrocortical membranes: 5-hydroxytryptamine receptors, fluidity, and inducible in vitro lipid peroxidation. J Neurochem 53:595–601.

Wang X, Arcuino G, Takano T, Lin J, Peng WG, Wan P, Li P, Xu Q, Liu QS, Goldman SA, et al. 2004. P2X7 receptor inhibition improves recovery after spinal cord injury. Nat Med 10:821–827.

White TD. 1977. Direct detection of depolarisation-induced release of ATP from a synaptosomal preparation. Nature 267:67–68.

Xia M, Zhu Y. 2011. Signaling pathways of ATP-induced PGE2 release in spinal cord astrocytes are EGFR transactivation-dependent. Glia 59: 664–674.